Nuclear Science and Techniques (2025) 36:24
https://doi.org/10.1007/s41365-024-01625-9

Effective nucleus-nucleus potentials for heavy-ion fusion reactions

Ning Wang[1,2] · **Jin-Ming Chen**[1] · **Min Liu**[1,2]

Received: 6 July 2024 / Revised: 14 September 2024 / Accepted: 18 September 2024 / Published online: 10 January 2025

Abstract
Based on the Skyrme energy density functional and reaction Q-value, this study proposed an effective nucleus-nucleus potential for describing the capture barrier in heavy-ion fusion processes. The 443 extracted barrier heights were well reproduced with a root-mean-square (RMS) error of 1.53 MeV, and the RMS deviations with respect to 144 time-dependent Hartree-Fock capture barrier heights were only 1.05 MeV. Coupled with the Siwek-Wilczyński formula, wherein three parameters were determined by the proposed effective potentials, the measured capture cross sections at energies around the barriers were reasonably well reproduced for several fusion reactions induced by nearly spherical nuclei as well as by nuclei with large deformations, such as ^{154}Sm and ^{238}U. The shallow capture pockets and small values of the average barrier radii resulted in the reduction of the capture cross sections for ^{52,54}Cr- and ^{64} Ni-induced reactions, which were related to the synthesis of new super-heavy nuclei.

Keywords Nucleus-nucleus potential · Fusion reactions · Superheavy nuclei · Capture cross sections

1 Introduction

The investigation of heavy-ion fusion reactions is important for the synthesis of new superheavy nuclei (SHN) [1–14] and extremely proton-rich nuclei [15–17] and the exploration of nuclear structures [18–22]. In the case of fusion reactions involving light and intermediate nuclei, approaches such as fusion-coupled channel calculations [22–24] and empirical barrier distribution methods [25–30] have been adopted to calculate capture (fusion) cross sections. These calculations are typically based on the static or dynamic nuclear potentials [31–37]. Static potentials are typically characterized using models, such as the liquid drop model, energy density functional or double-folding concept, coupled with a sudden approximation. The precise characterization of the nucleus-nucleus potential, particularly at short distances, is essential for comprehending the fusion mechanism.

A previous study [27] proposed a static entrance channel nucleus-nucleus potential to describe heavy-ion fusion reactions. They used the Skyrme energy density functional [38] combining the extended Thomas-Fermi (ETF) approach [39–41] and the sudden approximation for densities. By introducing an empirical barrier distribution composed of a combination of two-Gaussian (2G) functions to consider the dynamic effects in the fusion processes, the most probable barrier heights $V_B \approx 0.946B_0$ (with frozen barrier height B_0) and fusion excitation functions for various reactions can be described reasonably well [27, 28, 37]. Although certain measured fusion cross sections can be accurately reproduced, the realistic nucleus-nucleus potential in fusion processes, particularly at short distances, remains unclear. In addition, for certain fusion reactions related to the synthesis of super-heavy nuclei such as ^{64}Ni+^{238}U [42, 43], the extracted capture cross sections from the measured mass-total kinetic energy (TKE) distributions at energies above the Bass barrier [32] are significantly smaller than the predicted results of the classic fusion cross-section formula

This work was supported by the National Natural Science Foundation of China (Nos. 12265006, 12375129, U1867212), the Innovation Project of Guangxi Graduate Education (No. YCSWYCSW2022176), and the Guangxi Natural Science Foundation (2017GXNSFGA198001).

Ning Wang
wangning@gxnu.edu.cn

Min Liu
liumin@gxnu.edu.cn

1 Present Address: Department of Physics, Guangxi Normal University, Guilin 541004, China

2 Guangxi Key Laboratory of Nuclear Physics and Technology, Guilin 541004, China

$\sigma_{cap} = \pi R_B^2(1 - V_B/E_{c.m.})$ and the results of ETF+2G approach mentioned above. Owing to the measurements being highly time-consuming for reactions yielding elements 119 and 120, an accurate prediction of the capture cross sections and the evaporation residue (EvR) cross sections [44–48] is required.

In addition to static nuclear potentials, certain microscopic dynamics models [49], such as the time-dependent Hartree-Fock (TDHF) [50–52] and improved quantum molecular dynamics (ImQMD) model [53, 54], have also been widely adopted in studies focused on heavy-ion fusion reactions, wherein the time evolution of the densities of the composite system can be self-consistently described. Recently, the capture thresholds for 144 fusion reactions induced by nearly spherical nuclei have been systematically studied using TDHF calculations [55]. In conjunction with the Siwek-Wilczyński (SW) cross-section formula, which incorporates the classic cross-section formula by folding it with a Gaussian barrier distribution, the experimentally measured fusion cross sections at energies around the barriers can be reproduced well for certain fusion reactions such as ^{132}Sn+^{40,48}Ca. Moreover, the reaction Q-value can influence the fusion cross sections at sub-barrier energies in reactions with nearly spherical nuclei [55]. However, for fusion reactions involving strongly deformed nuclei, such as ^{154}Sm, ^{238}U and ^{243}Am, the effective consideration of both the Q-value and nuclear static deformations in the calculation of capture cross sections remains an unresolved issue. Furthermore, as microscopic TDHF calculations are extremely time-consuming, a time-saving nucleus-nucleus potential with high accuracy needs to be developed for the systematic study of fusion reactions.

In this work, we attempt to propose an effective nucleus-nucleus potential based on the Skyrme energy density functional (EDF) and the reaction Q-value for a systematic description of heavy-ion fusion reactions, particularly reaction systems with well-deformed nuclei.

2 Effective nucleus-nucleus potential

In this study, we first calculated the frozen nucleus-nucleus potential based on Skyrme EDF. The entrance-channel nucleus-nucleus potential $V(R)$ between two nuclei is expressed as [27, 56]

$$V(R) = E_{\text{tot}}(R) - E_1 - E_2, \tag{1}$$

where R is the center-to-center distance between the two fragments, $E_{\text{tot}}(R)$ denotes the total energy of the nuclear system, and E_1 and E_2 denote the energies of the reaction partners at an infinite distance. The total energy of a nuclear system can be expressed as an integral of the Skyrme EDF $\mathcal{H}(\mathbf{r})$ using the frozen density approximation:

$$E_{\text{tot}}(R) = \int \mathcal{H}[\rho_{1p}(\mathbf{r}) + \rho_{2p}(\mathbf{r} - \mathbf{R}), \rho_{1n}(\mathbf{r}) + \rho_{2n}(\mathbf{r} - \mathbf{R})]\, d\mathbf{r}. \tag{2}$$

The energies E_1 and E_2 are expressed as

$$E_1 = \int \mathcal{H}[\rho_{1p}(\mathbf{r}), \rho_{1n}(\mathbf{r})]\, d\mathbf{r}, \tag{3}$$

$$E_2 = \int \mathcal{H}[\rho_{2p}(\mathbf{r}), \rho_{2n}(\mathbf{r})]\, d\mathbf{r}, \tag{4}$$

where ρ_{1p}, ρ_{2p}, ρ_{1n} and ρ_{2n} are the frozen proton and neutron densities of the projectile and target described by spherically symmetric Fermi functions. When calculating the energies and corresponding densities of the reaction partners, Skyrme EDF with the parameter set SkM* [57] was adopted. Further, the extended Thomas-Fermi (ETF2) approach was used to describe both the kinetic energy density and spin-orbit density within the EDF.

Based on the entrance nucleus-nucleus potential $V(R)$, the frozen barrier height B_0 and depth of the capture pocket B_{cap} can be obtained [56]. The solid curve in Fig. 1a denotes the calculated $V(R)$ value for the reaction ^{40}Ca+^{144}Sm. Certain microscopic dynamics simulations have indicated that the frozen potential barrier is reduced in the fusion process owing to the dynamic deformations of the reaction partners and nucleon transfers. In a systematic study of ^{16}O-induced fusion using the ImQMD model in [54], the dynamic barrier height was lower than the frozen barrier height by approximately 5%.

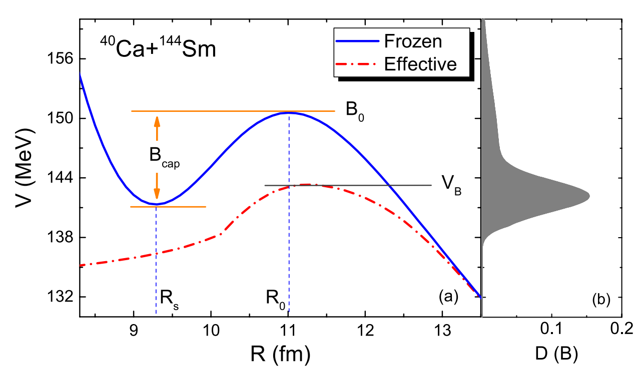

Fig. 1 **a** Nucleus-nucleus potential for ^{40}Ca + ^{144}Sm. The solid and dot-dashed curves denote the frozen and effective potentials, respectively. The short dashed lines denote the position of the frozen barrier R_0 and that of the pocket R_s. **b** Empirical barrier distribution for ^{40}Ca + ^{144}Sm proposed in [27]

To consider the influence of the dynamic effect, we proposed an effective potential (EP) $V_D(R)$ for fusion systems in the regions before the contact of the two nuclei:

$$V_D(R) = V(R)\left[1 - k\,\mathrm{erfc}\left(\frac{R - R_0}{s} - 1\right)\right], \quad (5)$$

with two parameters of $k = 0.027$ and $s = 1.0$ fm. With an increase in R between the two nuclei, the Coulomb excitation becomes negligible, and $V_D(R)$ is consequently close to $V(R)$. The dot-dashed curve in Fig. 1(a) denotes the effective nucleus-nucleus potential for ^{40}Ca+^{144}Sm. The barrier height was reduced from $B_0 = 150.57$ MeV to $V_B = 143.32$ MeV, and in the region $R > 13.5$ fm, one had $V_D(R) \approx V(R)$. Figure 1b shows the empirical barrier distribution with the superposition of the two-Gaussian functions proposed in [27]. Notably, the value of V_B approached the average barrier height owing to the distribution function. Further, the effective barrier radius R_B was slightly larger than the frozen radius R_0.

Following projectile-target contact at energies around the barrier height V_B, the frozen density approximation is no longer applicable because of the dynamic evolution of the neck. For a light fusion system, the compound nucleus is formed directly after the fusion barrier is overcome because the fission barrier is sufficiently high to render fission an improbable decay mode at incident energies close to the fusion barrier, and the potential V_D should approach $-Q$ when the distance between the two fragments becomes very small. For heavy systems, such as the reactions leading to SHN, the influence of quasi-fission becomes evident. This implies that the effective entrance-channel nucleus-nucleus potential $V_D(R)$ for heavy systems could be significantly larger than the value of $-Q$ at short distances. Moreover, nucleon transfer through the neck becomes an important method to form the compound nucleus, as described in the dinuclear system (DNS) model [45, 47, 58–61]. In the regions following the projectile-target contact, the effective potential (EP) is expressed as

$$V_D = V_s + \frac{\Delta U - Q - V_s}{1 + \exp[(R - R_2)/s]} + (V_1 - V_s)\exp\left(\frac{R - R_1}{s}\right), \quad (6)$$

where V_s and V_1 are the corresponding effective potentials obtained using Eq. (5) at distance $R = R_B - \Delta R$ and at the touching point $R = R_1$, respectively. Further, $\Delta R = R_0 - R_s$ and $R_2 = R_s/2$. R_0 and R_s are the barrier radius and position of the capture pocket in the frozen nucleus-nucleus potential $V(R)$, respectively (indicated by the dashed lines in Fig. 1). In this study, the touching point R_1 was considered as

$$R_1 = \begin{cases} R_0 & : \ \Delta R < 1.5 \text{ fm} \\ R_0 - \Delta R/2 & : \ \Delta R \geq 1.5 \text{ fm} \end{cases} \quad (7)$$

where $\Delta U = (V_B + Q) - (V_B^{\mathrm{sym}} + Q_{\mathrm{sym}})$ denotes the difference between the driving potential at the entrance channel and that of the corresponding symmetric system (i.e., the mass asymmetry of the projectile-target combination is approximately zero). According to the DNS model, the nucleon transfer is primarily governed by the driving potential. Here, we introduce the truncation for fusion reactions, that is, $\Delta U \geq 0$ and $V_s \geq -Q$, considering that the energy of the composite system after the projectile-target contact should be larger than that of the compound nucleus at its ground state for fusion reactions with heavy nuclei.

Figure 2 shows the calculated effective potentials for the reactions ^{16}O + ^{208}Pb, ^{48}Ca + ^{208}Pb, ^{30}Si + ^{238}U and ^{70}Zn + ^{209}Bi. The frozen nucleus-nucleus potentials (solid curves) are also presented for comparison. In a previous study [62], the fusion barrier parameters for 367 reaction systems were systematically extracted based on 443 datasets of measured fusion/fission cross sections. The green squares denote the extracted barrier heights [62]. As evident, the capture barrier heights V_B obtained from the effective potential (EP) were consistent with the experimental values. In this study, the calculated V_B with the proposed EP was systematically compared with the extracted barrier heights. The root-mean-square (RMS) deviations with respect to the 443 extracted barrier heights were 1.53 MeV, which is smaller than the Bass [32, 33] and BW91 [34] potentials. For ^{16}O + ^{208}Pb and ^{48}Ca + ^{208}Pb, the EP results approached the corresponding TDHF capture thresholds [55]. The RMS deviations with respect to the 144 capture barrier heights [55] predicted by TDHF calculations were only 1.05 MeV. Considering that microscopic TDHF calculations are extremely time-consuming, the proposed effective nucleus-nucleus potentials with similar accuracy would be useful for the systematic study of fusion reactions.

Figure 2 shows that for the intermediate fusion system ^{16}O + ^{208}Pb, the EP evidently decreased with a decrease in R after the projectile-target contact and gradually approached the value of $-Q = 46.5$ MeV. However, for the heavy fusion system ^{70}Zn + ^{209}Bi, the EP slightly decreased by $B_{\mathrm{cap}}^{\mathrm{D}} = 1.71$ MeV after projectile-target contact, and at very short distances, the potentials were even higher than V_B by approximately 2 MeV. This implied that the formation of the compound nuclei was a relatively slow process, and competition among fusion, quasi-fission, and deep-inelastic scattering was evident for this system. The gray lines in (b) and (d) denote the energies $V_E = 0.99 V_B$ below which elastic scattering was the dominant process. Figure 2(d) also indicates the difficulty in forming compound nuclei in the reaction ^{70}Zn + ^{209}Bi at energies lower than V_E based on the barrier penetration concept. This is because the potential barrier becomes

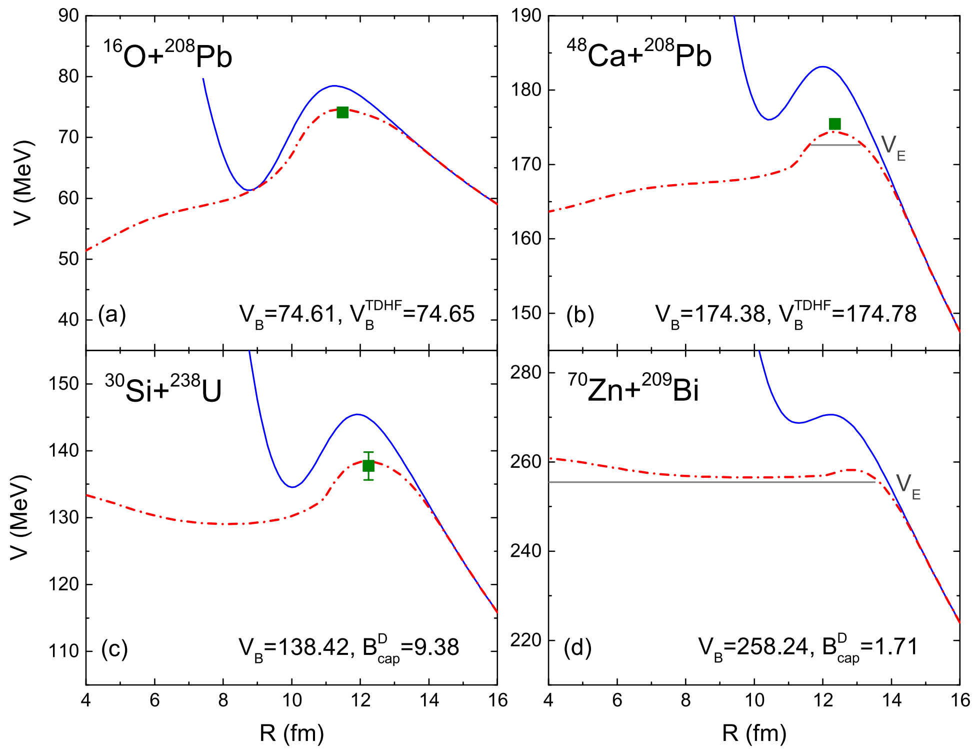

Fig. 2 Similar to the situation presented in Fig. 1(a), albeit for $^{16}O + ^{208}Pb$, $^{48}Ca + ^{208}Pb$, $^{30}Si+ ^{238}U$ and $^{70}Zn + ^{209}Bi$. The green squares denote the extracted barrier heights [62]. The gray lines in (b) and (d) indicate the energies of $V_E = 0.99V_B$. V_B^{TDHF} indicates the predicted capture barrier height in the TDHF calculations [55]

extremely thick. In addition, compared with the EP for $^{30}Si + ^{238}U$, wherein the depth of the capture pocket $B^D_{cap} = 9.38$ MeV was considerably larger than that of $^{70}Zn + ^{209}Bi$, the quasi-fission and deep-inelastic scattering events were considerably greater in $^{70}Zn + ^{209}Bi$ at energies around the capture barriers.

3 Capture cross sections

The couplings between the relative motion of colliding nuclei and the intrinsic degrees of freedom play an important role in heavy-ion fusion reactions. To consider these couplings, Stelson introduced the distribution of barrier heights $D(B)$ in the calculation of the fusion excitation function [63]. A well-known example is the Gaussian distribution of barrier heights predicted from different orientations of colliding nuclei that undergo slow deviations from sphericity [63]. In a previous study [26], an analytical cross-section formula was proposed for describing the capture excitation function at energies around the Coulomb barrier by Siwek-Wilczyńska and Wilczyński (SW) under the Gaussian distribution assumption,

$$\sigma_{cap}(E_{c.m.}) = \pi R_m^2 \frac{W}{\sqrt{2}E_{c.m.}}\left[X\mathrm{erfc}(-X) + \frac{1}{\sqrt{\pi}}\exp(-X^2)\right], \tag{8}$$

where $X = (E_{c.m.} - V_B)/\sqrt{2}W$, V_B and W denote the centroid and the standard deviation of the Gaussian function, respectively, and R_m denotes the average barrier radius, which is typically set as $R_m = R_B$. In this study, the average barrier radius was

$$R_m = \frac{\int (V_D - V_E)R\,dR}{\int (V_D - V_E)\,dR}. \tag{9}$$

This was calculated using the effective potential V_D at energies near the capture barrier height $E_{c.m.} = (1 \pm 0.01)V_B$. Notably, $R_m \approx R_B$ for most fusion systems (indicated by the positions of the green squares in Fig. 2). In contrast, for reaction systems with very shallow capture pockets, R_m is significantly smaller than R_B, which is discussed later.

For fusion reactions induced by heavy target nuclei with a quadrupole deformation of β_2, the range of barrier heights $\Delta B \propto \beta_2 V_B R_T/R_B$ owing to the different orientations of the deformed nuclei can be derived using an average target radius R_T [22]. Therefore, the V_B and β_2 dependences of W are expected for reactions with deformed nuclei. In contrast, the excitation energy of the compound nuclei (related to the reaction Q-value) at energies around the barrier in the reaction with deformed nuclei is typically larger than that with neighboring spherical nuclei. For example, the Q-value of the reaction $^{16}O+^{154}Sm$ is higher than that of $^{16}O+^{144}Sm$ by approximately 12 MeV (which is further discussed later). In addition, for heavy nuclei with large deformations, the excitation threshold ε_{th}, defined as the energy of the lowest excited state of the reaction partner, is typically very small, for example, $\varepsilon_{th} = 0.082$ MeV for ^{154}Sm and $\varepsilon_{th} = 0.045$ MeV for ^{238}U. The deformation parameter β_2 is model-dependent [29, 64]. Thus, it would be interesting to modify the barrier height effects with W having a Q-value and excitation threshold dependence.

Recently, the SW formula was applied to study the fusion excitation functions for reactions involving nearly spherical nuclei with three parameters determined by TDHF calculations [55]. The standard deviation of the Gaussian function W was observed to be related to the reaction Q-value and deformation effects. A relatively higher excitation energy at the capture position can facilitate stronger impacts on the dynamic deformations and nucleon transfer during the capture process, thereby broadening the width of the barrier distribution. Based on the concepts described in [55], we extended the expression of W to intermediate and heavy fusion reactions induced by nuclei with large deformations. The value of W for the fusion reactions induced by nuclei with large deformations is parameterized as

$$W = \frac{2}{3}W_0 + \frac{1}{3}W_1, \tag{10}$$

where $W_0 = 0.052(V_B + Q)$ for reactions induced by nearly spherical nuclei [55]. In a systematic study of the fusion barrier parameters, Chen et al. determined the value of $W \approx (0.014 + 0.135\lambda_B)V_B$ with the reduced de Broglie wavelength $\lambda_B = \hbar/\sqrt{2\mu V_B}$ [62]. Considering the systematic behavior of W, we write $W_1 = (0.048 + \eta\,\varepsilon_1/\varepsilon_2)V_B$. Here, $\eta = |A_1 - A_2|/(A_1 + A_2)$ denotes the mass asymmetry of the reaction system, where A_1 and A_2 are the mass numbers of the projectile and target, respectively. Further, ε_1 and ε_2 denote smaller and larger energies of the lowest excited states for the reaction partners, respectively. Simultaneously, we introduce a truncation of the value of W, that is, $W \le 2.5W_0$. Equation (10) shows that the V_B dependence of the barrier distribution width is considered in W_1 and the deformation effects are indirectly considered using the Q-value in W_0 and the energies of the lowest excited states in W_1.

Table 1 lists the calculated barrier parameters of the reactions under consideration. The barrier height V_B and average barrier radius R_m were obtained using Eqs. (5) and (9), respectively. The standard deviation of the Gaussian function W was obtained using Eq. (10). The reaction Q-value for unmeasured super-heavy system was obtained from the prediction of the Weizsäcker-Skyrme (WS4) mass model [65] with which the known masses can be reproduced with an RMS error of ~ 0.3 MeV [66] and the known α-decay energies of SHN can be reproduced with deviations smaller than 0.5 MeV [6, 12].

Figure 3 presents the effective potentials and fusion excitation functions for the reactions ^{16}O + ^{144,154}Sm. As shown in Fig. 3a, the calculated barrier heights were consistent with the experimental values. The fusion barrier height for the neutron-rich system ^{16}O + ^{154}Sm was lower than that of ^{16}O + ^{144}Sm by 1.09 MeV. At very short distances, the potentials approached the corresponding values of $-Q$. From Fig. 3b, it can be observed that the measured fusion cross sections for both ^{16}O + ^{144}Sm and ^{16}O + ^{154}Sm were well reproduced.

Table 1 Barrier parameters with the effective potential. Q denotes the reaction Q-value

Reaction	V_B (MeV)	W (MeV)	R_m (fm)	Q (MeV)
^{16}O+^{144}Sm	60.51	1.66	10.66	− 28.54
^{16}O+^{154}Sm	59.42	2.66	10.87	− 16.43
^{32}S+^{154}Sm	114.34	4.61	11.31	− 60.60
^{48}Ca+^{154}Sm	137.93	4.36	11.75	− 90.74
^{30}Si+^{238}U	138.42	4.51	12.24	− 93.01
^{48}Ca+^{238}U	191.19	3.95	12.71	− 160.78
^{52}Cr+^{232}Th	225.26	4.92	8.15	− 187.40
^{52}Cr+^{248}Cm	237.90	4.41	6.13	− 203.95
^{54}Cr+^{243}Am	235.49	3.68	5.98	− 207.20
^{64}Ni+^{238}U	263.37	3.22	5.42	− 238.61

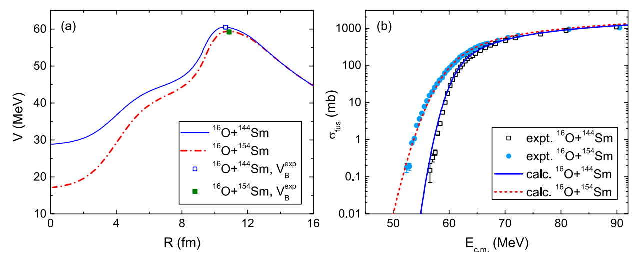

Fig. 3 **a** Similar to situation presented in Fig. 2, albeit for ^{16}O + ^{144,154}Sm. The data for the barrier heights are obtained from [62]. **b** Fusion excitation functions for ^{16}O + ^{144,154}Sm. The scattered symbols denote the experimental data taken from [67], and the curves denote the predicted results with Eq. (8)

Figure 4 shows the calculated capture excitation functions for reactions with the deformed nuclei ^{154}Sm and ^{238}U. The scattered symbols represent experimental data. The solid curves and short dashes denote the results of the effective potential coupled with the SW formula (Eq. 8) and the results of the ETF+2G approach [27], respectively. Notably, at energies near the capture barriers, the experimental data were reasonably well reproduced by both approaches. For ^{48}Ca + ^{238}U, the measured cross-sections at the sub-barrier energies were reproduced considerably better using the EP+SW approach. Here, we emphasize that the SW formula was obtained from the folding of the Gaussian barrier distribution and the classic over-barrier fusion cross-section expression, which is not applicable to deep sub-barrier energies because it does not consider the barrier penetration

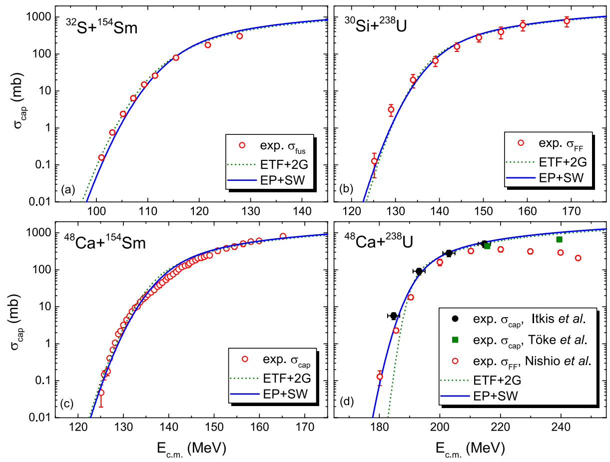

Fig. 4 Capture excitation functions for the reactions ^{32}S + ^{154}Sm [68], ^{30}Si + ^{238}U [69], ^{48}Ca + ^{154}Sm [70] and ^{48}Ca + ^{238}U [43, 71, 72]. The solid curves and short dashes denote the results of the effective potential coupled with the SW formula (Eq. 8) and the results of the empirical two-Gaussian (2G) barrier distribution approach [27], respectively

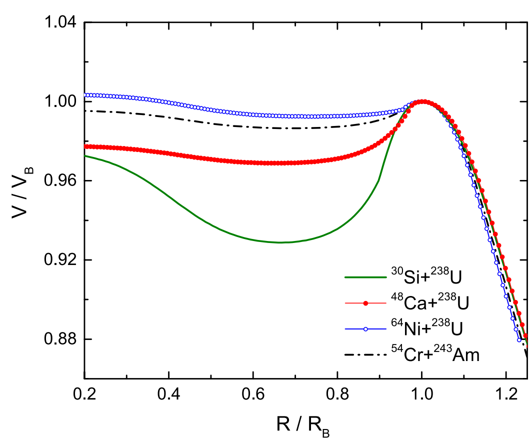

Fig. 5 Effective nucleus-nucleus potentials for ^{30}Si,^{48}Ca,^{64}Ni + ^{238}U and ^{54}Cr+^{243}Am

effect. Figures 3 and 4 indicate that the measured capture cross sections at energies near the barrier were well reproduced by the SW formula. Thus, the folding of a suitable barrier distribution plays a role in describing the capture cross sections around barrier energies. In addition, the Wong formula [31], which considers the quantum mechanical tunneling effect, was used to fold the two-Gaussian barrier distribution in the ETF+2G calculations. As evident, the results from the two approaches were similar for the reactions ^{32}S + ^{154}Sm, ^{30}Si + ^{238}U and ^{48}Ca + ^{154}Sm, which also indicates the importance of the barrier distribution.

Simultaneously, the proposed effective potential (EP) was tested to describe fusion reactions leading to the synthesis of superheavy nuclei. Figure 5 shows the calculated EP for the reactions ^{30}Si,^{48}Ca,^{64}Ni + ^{238}U and ^{54}Cr+^{243}Am. To observe the depth of the capture pockets more clearly, the potential and distance were scaled by V_B and R_B, respectively. Notably, the depths of the capture pockets significantly decreased with an increase in the product of the projectile-target charge numbers Z_1Z_2. Very recently, Yao et al. found that the yields of fission-like events in the measured mass-TKE distributions and the ratio of capture to deep-inelastic scattering events evidently decreased with a decrease in the depths of the capture pockets B_{cap} [56]. To understand the underlying physics, we studied the average barrier radius, R_m. Table 1 shows that for the reactions induced by ^{52,54}Cr and ^{64}Ni, the average barrier radii were significantly smaller than those of the other reactions, although the contact distances were larger. With smaller average barrier radii for reactions with ^{52,54}Cr and ^{64}Ni, the corresponding capture cross sections at the above barrier energies are expected to be reduced. Figure 6 shows the predicted capture cross-sections for the reactions ^{52}Cr+ ^{232}Th, ^{52}Cr+ ^{248}Cm, ^{54}Cr+^{243}Am and ^{64}Ni+ ^{238}U. The green dashed and blue solid curves denote the results predicted using the empirical 2G barrier distribution and EP+SW approaches, respectively. The solid circles denote the experimental data obtained from [43]. As evident, for ^{52}Cr+ ^{248}Cm and ^{64}Ni+ ^{238}U, the capture cross sections were significantly overpredicted by the ETF+2G approach. The dot-dashed curves denote the results with the ETF+2G approach but adopt the average barrier radius R_m in the calculations. When using R_m rather than R_B in the calculations, the capture cross sections at the above barrier energies were considerably better reproduced. The predicted capture cross sections at sub-barrier energies with the effective potential were evidently smaller than those with the 2G approach for ^{52,54}Cr-induced reactions. This implies that the predicted 2n EvR cross sections would be considerably smaller than those obtained using the ETF+2G approach for the reaction ^{54}Cr+^{243}Am.

4 Summary

Based on the frozen nucleus-nucleus potential from the Skyrme energy density functional, coupled with the extended Thomas-Fermi approach and sudden approximation of densities, this study proposed an effective approach to obtain the capture barrier heights and average barrier radii for heavy-ion fusion reactions. The 443 extracted barrier heights were well reproduced with an RMS error of 1.53 MeV. The effective potential results were very close to the corresponding TDHF capture thresholds for ^{16}O + ^{208}Pb and ^{48}Ca + ^{208}Pb. The RMS deviation with respect to the 144 capture barrier heights predicted using the TDHF calculations was only 1.05 MeV, which provides a useful

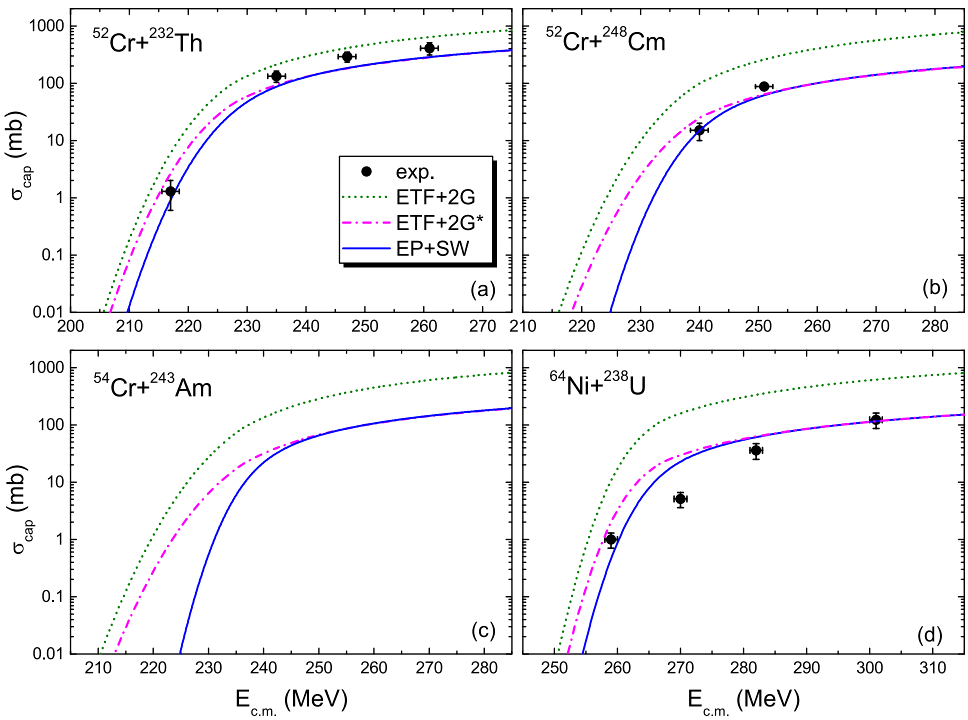

Fig. 6 (Color online) Similar to the situation presented in Fig. 4, albeit for ^{52}Cr+^{232}Th,^{248}Cm, ^{54}Cr+^{243}Am and ^{64}Ni+^{238}U. The dot-dashed curves denote the results with the 2G approach but with the average barrier radius R_m rather than R_B in the calculations. The data are obtained from [43]

balance between accuracy and computation cost, facilitating numerous fusion systems in a simple uniform manner. Combined with Siwek-Wilczyński formula, wherein the three parameters are determined by the proposed effective potentials, the measured capture cross sections at energies around the barriers were well reproduced for several fusion reactions induced by both spherical and well-deformed nuclei. The shallow capture pockets and small values of the average barrier radii led to the reduction of the capture cross sections for ^{52,54}Cr-and ^{64} Ni-induced reactions. Moreover, the decrease in the capture pocket depth for the heavy reaction system resulted in an increase in deep inelastic collisions at energies around the capture barrier, which consequently suppressed the production of the compound system.

Acknowledgements Certain data tables on the capture barrier heights are available at http://www.imqmd.com/fusion/.

Author contributions All authors contributed to the study conception and design. Material preparation, data collection, and analysis were performed by Ning Wang and Jin-Ming Chen. The first draft of the manuscript was written by Ning Wang, and all authors commented on previous versions of the manuscript. All authors read and approved the final manuscript.

Data availability The data that support the findings of this study are openly available in Science Data Bank at https://cstr.cn/31253.11.sciencedb.j00186.00441 and https://www.doi.org/10.57760/sciencedb.j00186.00441.

Declarations

Conflict of interest The authors declare that they have no conflict of interest.

References

1. S. Hofmann, G. Münzenberg, The discovery of the heaviest elements. Rev. Mod. Phys. **72**, 733–767 (2000). https://doi.org/10.1103/RevModPhys.72.733
2. S. Hofmann, F.P. Hessberger, D. Ackermanna et al., Properties of heavy nuclei measured at the GSI SHIP. Nucl. Phys. A **734**, 93–100 (2004). https://doi.org/10.1016/j.nuclphysa.2004.01.018
3. K. Morita, K. Morimoto, D. Kaji et al., Experiment on the synthesis of element 113 in the reaction ^{209}Bi(^{70}Zn, n)^{278}113. J. Phys. Soci. Japan **73**, 2593–2596 (2004). https://doi.org/10.1143/jpsj.73.2593
4. Y.T. Oganessian, V.K. Utyonkov, Y.V. Lobanov et al., Synthesis of the isotopes of elements 118 and 116 in the ^{249}Cf and ^{245}Cm+^{48}Ca fusion reactions. Phys. Rev. C **74**, 044602 (2006). https://doi.org/10.1103/PhysRevC.74.044602
5. Y.T. Oganessian, F.S. Abdullin, P.D. Bailey et al., Synthesis of a new element with atomic number $Z = 117$. Phys. Rev. Lett. **104**, 142502 (2010). https://doi.org/10.1103/PhysRevLett.104.142502
6. Y.T. Oganessian, V.K. Utyonkov, Superheavy nuclei from ^{48}Ca-induced reactions. Nucl. Phys. A **944**, 62–98 (2015). https://doi.org/10.1016/j.nuclphysa.2015.07.003
7. Y.T. Oganessian, V.K. Utyonkov, N.D. Kovrizhnykh et al., First experiment at the super heavy element factory: high cross section of ^{288}Mc in the ^{243}Am+^{48}Ca reaction and identification of the new

isotope ^{264}Lr. Phys. Rev. C **106**, L031301 (2022). https://doi.org/10.1103/PhysRevC.106.L031301
8. A. Sobiczewski, Y.A. Litvinov, M. Palczewski, Detailed illustration of the accuracy of currently used nuclear-mass models. Atom. Data Nucl. Data Tables **119**, 1–32 (2018). https://doi.org/10.1016/j.adt.2017.05.001
9. T. Tanaka, K. Morita, K. Morimoto et al., Study of quasielastic barrier distributions as a step towards the synthesis of superheavy elements with hot fusion reactions. Phys. Rev. Lett. **124**, 052502 (2020). https://doi.org/10.1103/PhysRevLett.124.052502
10. K. Pomorski, B. Nerlo-Pomorska, J. Bartel et al., Stability of superheavy nuclei. Phys. Rev. C **97**, 034319 (2018). https://doi.org/10.1103/PhysRevC.97.034319
11. G.G. Adamian, N.V. Antonenko, W. Scheid, Isotopic trends in the production of superheavy nuclei in cold fusion reactions. Phys. Rev. C **69**, 011601(R) (2004). https://doi.org/10.1103/PhysRevC.69.011601
12. Y.Z. Wang, S.J. Wang, Z.Y. Hou et al., Systematic study of α-decay energies and half-lives of superheavy nuclei. Phys. Rev. C **92**, 064301 (2015). https://doi.org/10.1103/PhysRevC.92.064301
13. Z. Wang, Z.Z. Ren, Predictions of the decay properties of the superheavy nuclei ^{293,294}119 and ^{294,295}120. Nucl. Tech. **46**, 080011 (2023). https://doi.org/10.11889/j.0253-3219.2023.hjs.46.080011. (**in Chinese**)
14. D.W. Guan, J.C. Pei, High quality microscopic nuclear masses of superheavy nuclei. Phys. Lett. B **851**, 138578 (2024). https://doi.org/10.1016/j.physletb.2024.138578
15. Z.Y. Zhang, Z.G. Gan, H.B. Yang et al., New isotope ^{220}Np: probing the robustness of the $N = 126$ shell closure in neptunium. Phys. Rev. Lett. **122**, 192503 (2019). https://doi.org/10.1103/PhysRevLett.122.192503
16. Z.Y. Zhang, H.B. Yang, M.H. Huang et al., New α-emitting isotope ^{214}U and abnormal enhancement of α-particle clustering in lightest uranium isotopes. Phys. Rev. Lett. **126**, 152502 (2021). https://doi.org/10.1103/PhysRevLett.126.152502
17. H.B. Zhou, Z.G. Gan, N. Wang et al., Lifetime measurement for the isomeric state in ^{213}Th. Phys. Rev. C **103**, 044314 (2021). https://doi.org/10.1103/PhysRevC.103.044314
18. R.G. Stokstad, Y. Eisen, S. Kaplanis et al., Effect of nuclear deformation on heavy-ion fusion. Phys. Rev. Lett. **41**, 465 (1978). https://doi.org/10.1103/PhysRevLett.41.465
19. V.V. Sargsyan, G.G. Adamian, N.V. Antonenko et al., Effects of nuclear deformation and neutron transfer in capture processes, and fusion hindrance at deep sub-barrier energies. Phys. Rev. C **84**, 064614 (2011). https://doi.org/10.1103/PhysRevC.84.064614
20. H.M. Jia, C.J. Lin, F. Yang et al., Extracting the hexadecapole deformation from backward quasi-elastic scattering. Phys. Rev. C **90**, 031601(R) (2014). https://doi.org/10.1103/PhysRevC.90.031601
21. L. Yang, C.J. Lin, H.M. Jia et al., Progress on nuclear reactions and related nuclear structure at low energies. Nucl. Tech. **46**, 080006 (2023). https://doi.org/10.11889/j.0253-3219.2023.hjs.46.080006. (**in Chinese**)
22. M. Dasgupta, D.J. Hinde, N. Rowley et al., Measuring barriers to fusion. Annu. Rev. Nucl. Part. Sci. **48**, 401–461 (1998). https://doi.org/10.1146/annurev.nucl.48.1.401
23. K. Hagino, N. Rowley, A.T. Kruppa, A program for coupled-channel calculations with all order couplings for heavy-ion fusion reactions. Comput. Phys. Commun. **123**, 143–152 (1999). https://doi.org/10.1016/S0010-4655(99)00243-X
24. C.H. Dasso, S. Landowne, CCFUS—a simplified coupled-channel code for calculation of fusion cross sections in heavy-ion reactions. Comput. Phys. Commun. **46**, 187–191 (1987). https://doi.org/10.1016/0010-4655(87)90045-2
25. V.I. Zagrebaev, Y. Aritomo, M.G. Itkis et al., Synthesis of superheavy nuclei: How accurately can we describe it and calculate the cross sections? Phys. Rev. C **65**, 014607 (2001). https://doi.org/10.1103/PhysRevC.65.014607
26. K. Siwek-Wilczyńska, J. Wilczyński, Empirical nucleus-nucleus potential deduced from fusion excitation functions. Phys. Rev. C **69**, 024611 (2004). https://doi.org/10.1103/PhysRevC.69.024611
27. M. Liu, N. Wang, Z.X. Li et al., Applications of Skyrme energy-density functional to fusion reactions spanning the fusion barriers. Nucl. Phys. A **768**, 80 (2006). https://doi.org/10.1016/j.nuclphysa.2006.01.011
28. N. Wang, M. Liu, Y.X. Yang, Heavy-ion fusion and scattering with Skyrme energy density functional. Sci. China Ser. G Phys. Mech. Astron. **52**, 1554 (2009). https://doi.org/10.1007/s11433-009-0205-z
29. B. Wang, K. Wen, W.J. Zhao et al., Systematics of capture and fusion dynamics in heavy-ion collisions. At. Data Nucl. Data Tables **114**, 281 (2017). https://doi.org/10.1016/j.adt.2016.06.003
30. C.L. Jiang, B.P. Kay, Heavy-ion fusion cross section formula and barrier height distribution. Phys. Rev. C **105**, 064601 (2022). https://doi.org/10.1103/PhysRevC.105.064601
31. C.Y. Wong, Interaction barrier in charged-particle nuclear reactions. Rev. Lett. **31**, 766 (1973). https://doi.org/10.1103/PhysRevLett.31.766
32. R. Bass, Fusion of heavy nuclei in a classical model. Nucl. Phys. A **231**, 45 (1974). https://doi.org/10.1016/0375-9474(74)90292-9
33. R. Bass, Fusion reactions: successes and limitations of a one-dimensional description. in *Lecture Notes in Physics*, vol. 117, (Springer, Berlin, 1980), p. 281. https://doi.org/10.1007/3-540-09965-4_23
34. R.A. Broglia, A. Winther, *Heavy Ion Reactions*. Frontiers in Physics, vol. **84**, (Addison-Wesley, 1991)
35. R.K. Puri, R.K. Gupta, Fusion barriers using the energy-density formalism: Simple analytical formula and the calculation of fusion cross sections. Phys. Rev. C **45**, 1837 (1992). https://doi.org/10.1103/PhysRevC.45.1837
36. P.W. Wen, C.J. Lin, H.M. Jia et al., New Coulomb barrier scaling law with reference to the synthesis of superheavy elements. Phys. Rev. C **105**, 034606 (2022). https://doi.org/10.1103/PhysRevC.105.034606
37. N. Wang, W. Scheid, Quasi-elastic scattering and fusion with a modified Woods-Saxon potential. Phys. Rev. C **78**, 014607 (2008). https://doi.org/10.1103/PhysRevC.78.014607
38. D. Vautherin, D.M. Brink, Hartree-Fock calculations with Skyrme's interaction. I. Spherical Nucl. Phys. Rev. C **5**, 626 (1972). https://doi.org/10.1103/PhysRevC.5.626
39. M. Brack, C. Guet, H.-B. Hakanson, Self-consistent semiclassical description of average nuclear properties-a link between microscopic and macroscopic models. Phys. Rep. **123**, 275 (1985). https://doi.org/10.1016/0370-1573(86)90078-5
40. J. Bartel, K. Bencheikh, Nuclear mean fields through self-consistent semiclassical calculations. Eur. Phys. J **A14**, 179 (2002). https://doi.org/10.1140/epja/i2000-10157-x
41. V.Y. Denisov, W. Noerenberg, Entrance channel potentials in the synthesis of the heaviest nuclei. Eur. Phys. J. A **15**, 375 (2002). https://doi.org/10.1140/epja/i2002-10039-3
42. E.M. Kozulin, G.N. Knyazheva, I.M. Itkis et al., Investigation of the reaction ^{64}Ni + ^{238}U being an option of synthesizing element 120. Phys. Lett. B **686**, 227 (2010). https://doi.org/10.1016/j.physletb.2010.02.041
43. M.G. Itkis, G.N. Knyazheva, I.M. Itkisa et al., Experimental investigation of cross sections for the production of heavy and superheavy nuclei. Eur. Phys. J. A **58**, 178 (2022). https://doi.org/10.1140/epja/s10050-022-00806-7
44. N. Wang, J.L. Tian, W. Scheid, Systematics of fusion probability in "hot" fusion reactions. Phys. Rev. C. **84**, 061601(R) (2011). https://doi.org/10.1103/PhysRevC.84.061601

45. G.G. Adamian, N.V. Antonenko, H. Lenske et al., Predictions of identification and production of new superheavy nuclei with Z=119 and 120. Phys. Rev. C **101**, 034301 (2020). https://doi.org/10.1103/PhysRevC.101.034301
46. K.V. Novikov, E.M. Kozulin, G.N. Knyazheva et al., Investigation of fusion probabilities in the reactions with ^{52,54}Cr,^{64}Ni, and ^{68}Zn ions leading to the formation of Z=120 superheavy composite systems. Phys. Rev. C **102**, 044605 (2020). https://doi.org/10.1103/PhysRevC.102.044605
47. J.X. Li, H.F. Zhang, Possibility to synthesize Z>118 superheavy nuclei with ^{54}Cr projectiles. Phys. Rev. C **108**, 044604 (2023). https://doi.org/10.1103/PhysRevC.108.044604
48. S. Madhu, H.C. Manjunatha, N. Sowmya et al., Cr induced fusion reactions to synthesize superheavy elements. Nucl. Sci. Tech. **35**, 90 (2024). https://doi.org/10.1007/s41365-024-01449-7
49. M.H. Zhang, Y.H. Zhang, J.J. Li et al., Progress in transport models of heavy-ion collisions for the synthesis of superheavy nuclei. Nucl. Tech. **46**, 080014 (2023). https://doi.org/10.11889/j.0253-3219.2023.hjs.46. (**in Chinese**)
50. J.A. Maruhn, P.G. Reinhard, P.D. Stevenson et al., Spin-excitation mechanisms in Skyrme-force time-dependent Hartree-Fock calculations. Phys. Rev. C **74**, 027601 (2006). https://doi.org/10.1103/PhysRevC.74.027601
51. L. Guo, J.A. Maruhn, P.G. Reinhard, Boost-invariant mean field approximation and the nuclear Landau-Zener effect. Phys. Rev. C **76**, 014601 (2007). https://doi.org/10.1103/PhysRevC.76.014601
52. C. Simenel, Challenges in description of heavy-ion collisions with microscopic time-dependent approaches. J. Phys. G Nucl. Part. Phys. **41**, 094007 (2014). https://doi.org/10.1088/0954-3899/41/9/094007
53. N. Wang, L. Ou, Y.X. Zhang, Z.X. Li, Microscopic dynamics simulations of heavy-ion fusion reactions induced by neutron-rich nuclei. Phys. Rev. C **89**, 064601 (2014). https://doi.org/10.1103/PhysRevC.89.064601
54. N. Wang, K. Zhao, Z.X. Li, Systematic study of ^{16}O-induced fusion with the improved quantum molecular dynamics model. Phys. ReV. C **90**, 054610 (2014). https://doi.org/10.1103/PhysRevC.90.054610
55. H. Yao, H. Yang, N. Wang, Systematic study of capture thresholds with time dependent Hartree-Fock theory. Phys. Rev. C **110**, 014602 (2024). https://doi.org/10.1103/PhysRevC.110.014602
56. H. Yao, C. Li, H.B. Zhou, N. Wang, Distinguishing fission-like events from deep-inelastic collisions. Phys. Rev. C **109**, 034608 (2024). https://doi.org/10.1103/PhysRevC.109.034608
57. J. Bartel, Ph. Quentin, M. Brack et al., Towards a better parametrisation of Skyrme-like effective forces: A critical study of the SkM force. Nucl. Phys. A **386**, 79 (1982). https://doi.org/10.1016/0375-9474(82)90403-1
58. G.G. Adamian, N.V. Antonenko, W. Scheid, V.V. Volkov, Treatment of competition between complete fusion and quasifission in collisions of heavy nuclei. Nucl. Phys. A **627**, 361 (1997). https://doi.org/10.1016/S0375-9474(97)00605-2
59. N. Wang, E.G. Zhao, W. Scheid, S.G. Zhou, Theoretical study of the synthesis of superheavy nuclei with Z=119 and 120 in heavy-ion reactions with trans-uranium targets. Phys. Rev. C **85**, 041601R (2012). https://doi.org/10.1103/PhysRevC.85.041601
60. L. Zhu, J. Su, F.S. Zhang, Influence of the neutron numbers of projectile and target on the evaporation residue cross sections in hot fusion reactions. Phys. Rev. C **93**, 064610 (2016). https://doi.org/10.1103/PhysRevC.93.064610
61. M.H. Zhang, Y.H. Zhang, Y. Zou et al., Possibilities for the synthesis of Superheavy element in $Z = 121$ fusion reactions. Nucl. Sci. Tech. **35**, 95 (2024). https://doi.org/10.1007/s41365-024-01452-y
62. Y. Chen, H. Yao, M. Liu et al., Systematic study of fusion barriers with energy dependent barrier radius. Atom. Data Nucl. Data Tables **154**, 101587 (2023). https://doi.org/10.1016/j.adt.2023.101587
63. P. Stelson, Neutron flow between nuclei as the principal enhancement mechanism in heavy-ion sub-barrier fusion. Phys. Lett. B **205**, 190 (1988). https://doi.org/10.1016/0370-2693(88)91647-4
64. N. Wang, T. Li, Nuclear deformation energies with the Weizsäcker-Skyrme mass model. Acta Phys. Polo. B Supp. **12**, 715 (2019). https://doi.org/10.5506/APhysPolBSupp.12.715
65. N. Wang, M. Liu, X.Z. Wu, J. Meng, Surface diffuseness correction in global mass formula. Phys. Lett. B **734**, 215 (2014). https://doi.org/10.1016/j.physletb.2014.05.049
66. X.H. Wu, Y.Y. Lu, P.W. Zhao, Multi-task learning on nuclear masses and separation energies with the kernel ridge regression. Phys. Lett. B **834**, 137394 (2022). https://doi.org/10.1016/j.physletb.2022.137394
67. J.R. Leigh, M. Dasgupta, D.J. Hinde et al., Barrier distributions from the fusion of oxygen ions with ^{144,148,154}Sm and ^{186}W. Phys. Rev. C **52**, 3151 (1995). https://doi.org/10.1103/PhysRevC.52.3151
68. P.R.S. Gomes, I.C. Charret, R. Wanis et al., Fusion of ^{32}S+^{154}Sm at sub-barrier energies. Phys. Re. C **49**, 245 (1994). https://doi.org/10.1103/PhysRevC.49.245
69. K. Nishio, H. Ikezoe, I. Nishinaka et al., Evidence for quasifission in the sub-barrier reaction of ^{30}Si+^{238}U. Phys. Rev. C **82**, 044604 (2010). https://doi.org/10.1103/PhysRevC.82.044604
70. M. Trotta, A.M. Stefanini, S. Beghini et al., Fusion hindrance and quasi-fission in ^{48}Ca induced reactions. Eur. Phys. J. A **25**, 615 (2005). https://doi.org/10.1140/epjad/i2005-06-084-2
71. K. Nishio, S. Mitsuoka, I. Nishinaka et al., Fusion probabilities in the reactions Ca+U at energies around the Coulomb barrier. Phys. Rev. C **86**, 034608 (2012). https://doi.org/10.1103/PhysRevC.86.034608
72. J. Töke, B. Bock, G.X. Dai et al., Quasi-fission-The mass-drift mode in heavy-ion reactions. Nucl. Phys. A **440**, 327 (1985). https://doi.org/10.1016/0375-9474(85)90344-6